J Nanopart Res (2014) 16:2662
DOI 10.1007/s11051-014-2662-1

RESEARCH PAPER

# Evaluation of the efficiency of tumor and tissue delivery of carrier-mediated agents (CMA) and small molecule (SM) agents in mice using a novel pharmacokinetic (PK) metric: relative distribution index over time (RDI-OT)

**Andrew J. Madden · Sumit Rawal · Katie Sandison · Ryan Schell · Allison Schorzman · Allison Deal · Lan Feng · Ping Ma · Russell Mumper · Joseph DeSimone · William C. Zamboni**

Received: 19 June 2014 / Accepted: 18 September 2014 / Published online: 11 October 2014


**Abstract** The pharmacokinetics (PK) of carrier-mediated agents (CMA) is dependent upon the carrier system. As a result, CMA PK differs greatly from the PK of small molecule (SM) drugs. Advantages of CMAs over SMs include prolonged circulation time in plasma, increased delivery to tumors, increased antitumor response, and decreased toxicity. In theory, CMAs provide greater tumor drug delivery than SMs due to their prolonged plasma circulation time. We sought to create a novel PK metric to evaluate the efficiency of tumor and tissue delivery of CMAs and SMs. We conducted a study evaluating the plasma, tumor, liver, and spleen PK of CMAs and SMs in mice bearing subcutaneous flank tumors using standard PK parameters and a novel PK metric entitled relative distribution over time (RDI-OT), which measures efficiency of delivery. RDI-OT is defined as the ratio of tissue drug concentration to plasma drug concentration at each time point. The standard concentration versus time area under the curve values (AUC) of CMAs were higher in all tissues and plasma compared with SMs. However, 8 of 17 SMs had greater tumor RDI-OT $AUC_{0-last}$ values than their CMA comparators and all SMs had greater tumor RDI-OT $AUC_{0-6\ h}$ values than their CMA comparators. Our results indicate that in mice bearing flank tumor xenografts, SMs distribute into tumor more efficiently than CMAs. Further research in additional tumor models that may more closely resemble tumors seen in patients is needed to determine if our results are consistent in different model systems.

**Electronic supplementary material** The online version of this article (doi:10.1007/s11051-014-2662-1) contains supplementary material, which is available to authorized users.

A. J. Madden · S. Rawal · K. Sandison · R. Schell · A. Schorzman · W. C. Zamboni (✉)
Division of Pharmacotherapy and Experimental Therapeutics, University of North Carolina at Chapel Hill (UNC) Eshelman School of Pharmacy, 120 Mason Farm Road, Suite 1013, CB 7361, Chapel Hill, NC 27599-7361, USA
e-mail: zamboni@email.unc.edu

A. Deal · J. DeSimone · W. C. Zamboni
Lineberger Comprehensive Cancer Center, University of North Carolina, Chapel Hill, NC, USA

A. Deal
UNC Lineberger Biostatistics Core Facility, University of North Carolina, Chapel Hill, NC, USA

L. Feng · P. Ma
Center for Nanotechnology in Drug Delivery, Division of Molecular Pharmaceutics, UNC Eshelman School of Pharmacy, Chapel Hill, NC, USA

R. Mumper
UNC Eshelman School of Pharmacy, University of North Carolina Chapel Hill, Chapel Hill, NC, USA

J. DeSimone
Department of Pharmaceutical Sciences, University of North Carolina, Chapel Hill, NC, USA

J. DeSimone
Department of Chemistry, University of North Carolina, Chapel Hill, NC, USA

**Keywords** Nanoparticles · Pharmacokinetics · Drug delivery · Chemotherapy · Nanomedicine

## Introduction

There has been a great increase in the number of carrier-mediated agents (CMA) being studied for targeted drug delivery in the past 15 years (Ge et al. 2011). CMAs include liposomes, non-liposomal nanoparticles, and conjugated agents. Liposomes are vesicles that consist of a phospholipid bilayer with drug contained in the aqueous center or embedded in the phospholipid bilayer. Liposomes may be either conventional or stabilized with polyethylene glycol (PEGylated), which greatly increases their circulation time (Zamboni 2005). Non-liposomal nanoparticles include solid lipid nanoparticles and polymeric nanoparticles. Solid lipid nanoparticles consist of a microemulsion which has drug loaded in the lipid portion (Ma et al. 2013). Polymeric nanoparticles consist of a polymeric matrix that can be molded into different shapes and sizes which has drug embedded within Chu et al. 2013). Conjugated agents consist of a small molecule (SM) drug which is linked to a polymer (Walsh et al. 2012). The theoretical advantages of CMAs include greater solubility, longer duration of exposure, selective delivery of encapsulated drug to the site of action, superior therapeutic index, and the potential to overcome resistance associated with anticancer agents (Drummond et al. 1999; Papahadjopoulos et al. 1991; Zamboni 2005, 2008). The potential advantages of CMAs over traditional SM drugs have led to interest in the development of carrier mediated formulations of chemotherapeutic agents.

The pharmacokinetics (PK) of CMAs is dependent upon the properties of the carrier and not the SM drug until the drug is released from the carrier (Zamboni 2005, 2008). CMAs act as prodrugs and are not active until the SM drug is released from the carrier. Once the SM drug is released from the carrier, its PK is the same as the non-carrier mediated formulation of that drug (Zamboni 2008). Nomenclature has been created to describe the different states of CMAs. The term encapsulated or conjugated is used to describe the drug still bound to or within the carrier. The term released drug describes the drug after it has been released from the carrier. The term sum total is used to describe the sum of both encapsulated and released drug (Zamboni 2005). While SM drugs are typically metabolized by the liver or eliminated by the kidney, it is thought that CMAs are cleared mainly through the cells of the mononuclear phagocyte system (MPS) (Caron et al. 2012; Laverman et al. 2001; Litzinger et al. 1994; Zamboni 2005). The MPS comprises cells such as macrophages and monocytes which phagocytose pathogens and dead cells to remove them from the body (Vonarbourg et al. 2006). Cells of the MPS take up CMAs and transport them to the organs associated with the MPS such as the liver and spleen, where they are further degraded and removed from the body. Due to the complex nature of CMA detailed PK and biodistribution studies in animals and patients need to be performed to evaluate their disposition (Zamboni 2008).

Tumor targeting by non-actively targeted CMAs is believed to be a passive process via the enhanced permeability and retention (EPR) effect (Alonso 2004; Matsumura and Maeda 1986). When SM chemotherapeutic drugs are administered intravenously, they quickly distribute to most tissues of the

J. DeSimone · W. C. Zamboni
Carolina Center of Cancer Nanotechnology Excellence, University of North Carolina, Chapel Hill, NC, USA

J. DeSimone
Department of Pharmacology, Eshelman School of Pharmacy, University of North Carolina, Chapel Hill, NC, USA

J. DeSimone
Institute for Nanomedicine, University of North Carolina, Chapel Hill, NC, USA

J. DeSimone
Institute for Advanced Materials, University of North Carolina, Chapel Hill, NC, USA

W. C. Zamboni
UNC Institute for Pharmacogenomics and Individualized Therapy, Chapel Hill, NC, USA

W. C. Zamboni
North Carolina Medical Innovation Network, Chapel Hill, NC, USA

body, and rapidly diffuse out of these tissues. This leads to low drug exposure in the tumor and unnecessary exposure of healthy tissue to cytotoxic agents. However, CMAs are not able to diffuse from the peripheral circulation into normal tissues because of their relatively large size, which means that most of the dose remains in the central compartment (the blood stream) (Duncan 1999; Zamboni 2005). While CMAs are not able to enter normal tissues, differences in tumor vascularity and biology allow CMAs to enter and accumulate in tumors. Tumor vasculature differs from the vasculature of normal tissues in that it is abnormally leaky, which allows CMAs to extravasate into the extracellular fluid of tumors (Duncan 1999). In addition to leaky vasculature, tumors also have impaired lymphatic function, which decreases the clearance of macromolecules from tumor (Matsumura and Maeda 1986). In theory, this phenomenon is known as the EPR effect and it allows CMA to accumulate for extended durations in tumors (Alonso 2004; Matsumura and Maeda 1986).

CMAs can be engineered to achieve much longer plasma circulation times than SM (Drummond et al. 1999). It has been shown that steric stabilization of CMAs reduces their rate of uptake by the MPS, though the mechanism behind this phenomenon is unclear (Zamboni 2005). Decreasing the rate of uptake of CMAs by the MPS leads to a decreased plasma clearance and thus a longer residence time in the plasma after administration (Drummond et al. 1999). CMAs that have been stabilized by PEGylation or conjugation with other polymers can achieve plasma half-lives of >40 h (Drummond et al. 1999). Theoretically, the EPR effect, combined with the long plasma circulation times seen with sterically stabilized agents, would result in a more efficient delivery of CMAs to tumors than is seen with SMs.

Standard PK parameters and metrics used for SMs have been used to describe CMAs. However, these standard PK parameters may not provide important and detailed information that describes SMs and CMAs, especially as related to efficiency of tumor delivery. This study will evaluate the PK properties of SMs and CMAs in mice with subcutaneous xenograft and syngenetic tumors. The efficiency of CMAs and SMs agents will be evaluated by a new PK metric, the relative distribution over time (RDI-OT), which was created for this analysis.

## Materials and methods

### Study design

A computerized literature search was conducted using the MEDLINE database to find PK studies of CMAs and SMs given intravenously in mice with xenograft or synergistic subcutaneous tumors implanted on the flank of mice. The bibliography of studies and literature reviews identified in the MEDLINE search were also used to identify additional studies. Inclusion factors for the study were that the paper must report the concentration versus time profile of the CMA and its comparative SM in plasma and tumor, the mouse model used, the tumor line, and dose of each agent administered.

### Data summary

Plasma and tumor concentration versus time profiles were obtained from tables and concentration versus time curves reported in the results sections of selected articles. Liver and spleen concentration versus time profiles were also obtained when available, as these are organs of the MPS where the majority of the CMA agents depot. Graph digitizing software (GetData Graph Digitizer v. 2.24) was used to convert concentration versus time curves to raw data.

### PK analysis

The areas under the concentration versus time curves (AUC) for plasma, tumor, liver, and spleen from 0 h to time last and from 0 to 6 h were calculated by noncompartmental analysis for each CMA and SM agent using Phoenix WinNonlin version 6.2 (Pharsight, St. Louis, MO) The concentration versus time profile was also used to calculate a new PK metric entitled the relative distribution index over time (RDI-OT). The RDI-OT is defined as the concentration of drug in tumor or tissue divided by the concentration of drug in the plasma at the corresponding time point. Figure 1 illustrates an example RDI-OT calculation. A theoretical tumor RDI-OT value at 6 h has been calculated by dividing the tumor drug concentration at 6 h by the plasma drug concentration at 6 h. The RDI-OT value for each PK time point can be calculated using this method. The RDI-OT values were then plotted against time to generate an RDI-OT versus

time curve. For each agent, the RDI-OT values for tumor, liver, and spleen were calculated at all PK time points and then plotted against time. The area under the RDI-OT versus time curves (RDI-OT AUC) from 0 h to time last and from 0 to 6 h were calculated by noncompartmental analysis using Phoenix WinNonlin version 6.2. RDI-OT AUC is different from the ratio of tissue or tumor AUC to plasma AUC because there are no tumor, tissue, or plasma AUC values used in the calculation of RDI-OT. Rather, the ratio of drug concentration in tumor or tissue to drug concentration in plasma is calculated at each individual time point then the values are plotted against time to create an RDI-OT curve.

The following PK parameters were calculated for all agents: standard plasma and tumor AUCs, ratio of standard plasma AUC to standard tumor AUC, ratio of (SM tumor AUC/plasma AUC) to (CMA tumor AUC/plasma AUC), the tumor RDI-OT AUC from 0 h to time last, the ratio of SM tumor RDI-OT AUC from 0 h to time last to its comparative CMA tumor RDI-OT AUC from 0 h to time last, the tumor RDI-OT AUC from 0 to 6 h, the ratio of SM tumor RDI-OT AUC from 0 to 6 h to its comparative CMA tumor RDI-OT AUC from 0 to 6 h, the liver RDI-OT AUC from 0 h to time last, the liver RDI-OT AUC from 0 to 6 h, the spleen RDI-OT AUC from 0 h to time last, and the spleen AUC RDI-OT from 0 to 6 h.

### Statistical analysis

The mean, standard deviation, median, and range were calculated for each PK parameter. The correlation of RDI-OT values with tissue and plasma AUC ratios was evaluated using Pearson's correlation coefficient (R). Wilcoxon Rank Sum tests were performed to compare distributions of SM RDI-OT AUC to CMA RDI-OT AUC. Differences in RDI-OT AUC distributions were determined to be statistically significant for $P < 0.05$.

## Results

### Data summary

Our search identified 12 articles that met the inclusion factors for the study. In addition, the results of 3

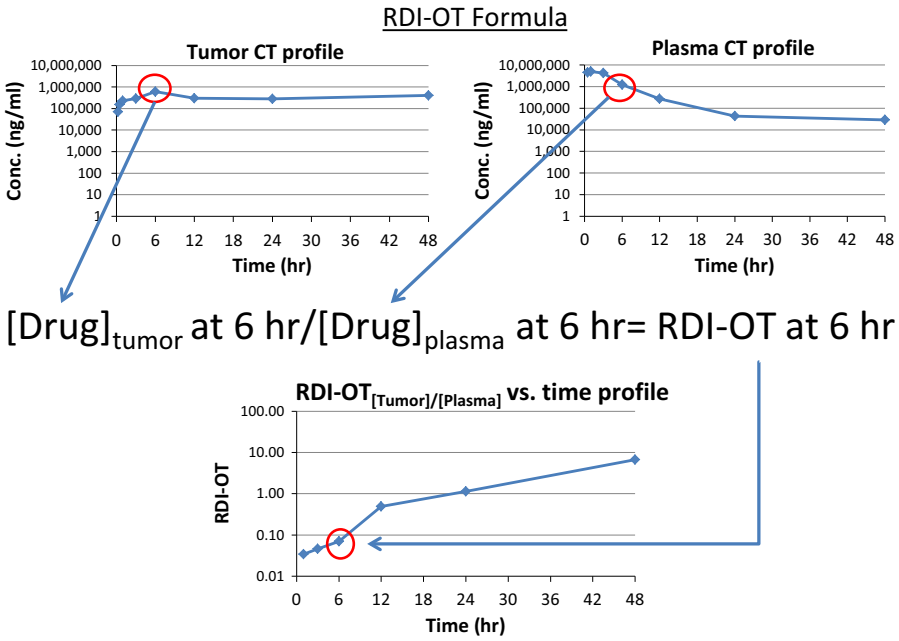


**Fig. 1** Illustration of a theoretical relative distribution index-over time (RDI-OT) calculation. Plot on the *top left* is a theoretical tumor drug concentration versus time profile. Plot on the *top right* is a theoretical plasma drug concentration versus time profile. The 6 h RDI-OT value is calculated by dividing the 6 h tumor drug concentration by the 6 h plasma drug concentration. The RDI-OT is calculated for each time point. RDI-OT values can then be plotted against time (plot on the *bottom left*) and the AUC of the RDI-OT *curve* can be calculated as a measure of efficiency of drug delivery

previously unpublished studies were included. In these 15 studies, PK data were available for 17 CMAs and 15 SMs (Chu et al. 2013; Desjardins et al. 2001; Farrell 2011; Feng et al. 2013; Forssen et al. 1992; Gabizon et al. 1997; Konishi et al.2012; Ma et al. 2013; Mayer et al. 1990; Sapra et al. 2008; Takahashi et al. 2010; Valery et al. 1999; Walsh et al. 2012; Zamboni et al. 2004, 2007). Two of the studies compared two separate CMA formulations to a single SM formulation, which explains why there were data available for 2 more CMA than SM (Chu et al. 2013; Farrell 2011). A summary of the mouse model used in each study, the CMAs and their comparative SM agents, and the tumor line for each study is presented in Table 1. There were five non-liposomal nanoparticles, six PEGylated liposomes, three non-PEGylated liposomes, and three conjugate agents included in the study. Additionally, we have included a summary of the physiochemical properties (size, shape, zeta potential, composition, and surface coating) of all CMAs in Supplemental Table 1.

## Standard PK results

The plasma concentration versus time profiles for all agents are shown in Fig. 2. The agents have been

**Table 1** Summary of CMA, SM, murine strain, and tumor models

| CMA/comparative SM | CMA type | Mouse strain | Tumor line | Reference |
|---|---|---|---|---|
| SPI-077/cisplatin | PEGylated liposome | Female C57Bl/6 | B16 murine melanoma | Zamboni et al. (2004) |
| S-CKD602/CKD-602 | PEGylated liposome | Female C·B-17 SCID | A375 human melanoma | Zamboni et al. (2007) |
| XMT-1001/CPT-11 | Conjugated agent | Female athymic nude (*nu/nu*) | HT-29 human colon carcinoma | Walsh et al. (2012) |
| PRINT-docetaxel/docetaxel | Non-liposomal nanoparticle | Female C·B-17 SCID | SKOV-3 human ovarian carcinoma | Chu et al. (2013) |
| CSO201/cisplatin | PEGylated liposome | Female nu/nu | KB nasopharyngeal carcinoma | Farrell (2011) |
| Folate-CSO201/cisplatin | Folate-Labeled PEGylated liposome | Female nu/nu | KB nasopharyngeal carcinoma | Farrell (2011) |
| IHL-305/CPT-11 | PEGylated liposome | BALB/cA Jcl-*nu/nu* | ES-2 ovarian clear cell carcinoma | Konishi et al. (2012) |
| BTM-docetaxel/docetaxel | Non-liposomal nanoparticle | Female BALB/c | 4T1 | Feng et al. (2013) |
| BTM-paclitaxel/paclitaxel | Non-liposomal nanoparticle | Female BALB/c | 4T1 | Ma et al. (2013) |
| NK012/SN-38 | Conjugated agent | Female BALB/c | HT-29 colon carcinoma | Takahashi et al. (2010) |
| SP1049C/doxorubicin | Conjugated agent | Female C57Bl/6 | s.c. 3LL-M27 | Alakhov et al. (1999) |
| ENZ-2208/SN-38 | Conjugated agent | Female BALB/c | MX-1 breast carcinoma | Sapra et al. (2008) |
| PLD/doxorubicin | PEGylated liposome | Female BALB/c | A375 | Gabizon et al. (1997) |
| Liposomal daunorubicin/ daunorubicin | Conventional liposome | Female $CD2F_1$ | P-1798 lymphosarcoma solid tumors | Forssen et al. (1992) |
| Liposomal doxorubicin/ doxorubicin | Conventional liposome | Male DD/S | SC115 mammary carcinoma | Mayer et al. (1990) |
| OSI-211/lurtotecan | Conventional liposome | Female nu/nu | KB (head/neck) | Desjardins et al. (2001) |

All SM docetaxel is Taxotere®. SM paclitaxel is Taxol®. Liposomal daunorubicin is DaunoXome®. Liposomal doxorubicin is Myocet®

*PLD* pegylated liposomal doxorubicin, *SM* small molecule, *CMA* carrier mediated agent

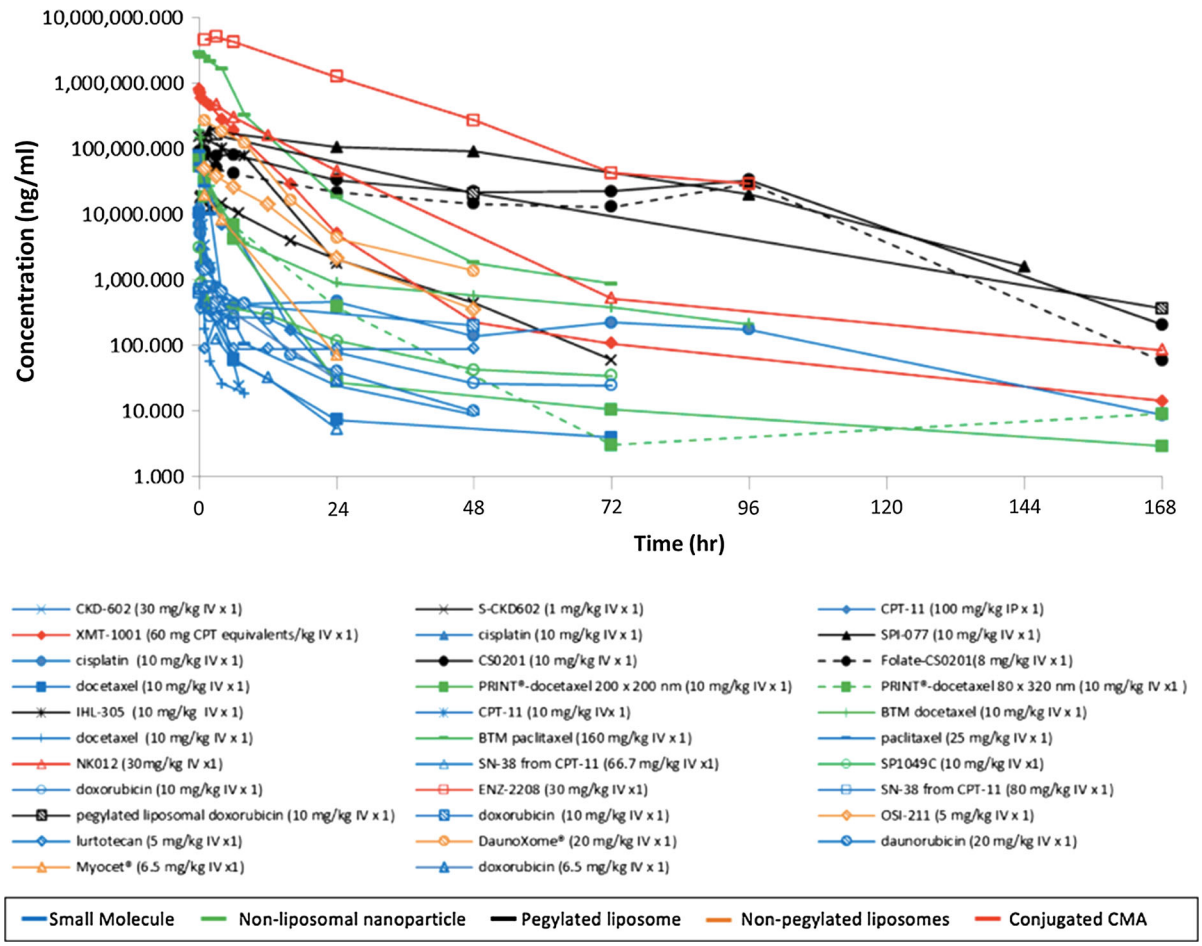


**Fig. 2** Comparison of concentration versus time profiles in plasma following the administration of CMAs and SMs. The plasma concentration versus time curves for all agents identified in the study. *Curves* with corresponding *symbols* indicate that those agents are from the same study. *Blue curves* represent SMs, *green curves* represent non-liposomal nanoparticles, *black curves* represent PEGylated lipsomes, *orange curves* represent non-PEGylated liposomes, and *red curves* represent conjugated agents. (Color figure online)

classified by CMA subtype, with SMs being put in their own class. Conjugated agents achieved the greatest plasma concentrations, followed by PEGylated liposomes. Non-liposomal nanoparticle and conventional liposomes had the lowest plasma concentrations of the CMAs. SMs had the lowest plasma concentrations of all agents. Predictably, SMs were cleared quickly with most agents being undetectable after 24 h. One exception to the fast clearance of SMs was cisplatin where total cisplatin (protein bound + unbound drug) was detectable at 168 h after administration. This can be explained by the fact that cisplatin is highly and covalently bound to albumin and therefore its prolonged exposure in the plasma is indicative of albumin clearance (Oberoi et al. 2012).

The physiochemical properties of the CMAs had an effect on the plasma PK of the CMAs. The major factors affecting plasma PK were composition and surface coating. In general, particles that were coated with PEG achieved much higher plasma concentrations and had much longer circulation times. In addition, conjugated agents achieved higher plasma concentrations and circulated longer than agents composed of lipids or polymers that were not PEGylated. No other physiochemical properties were associated with the plasma PK of the agents evaluated.

The tumor concentration versus time profiles of all agents included in the analysis are shown in Fig. 3. As reported with the plasma concentration profiles, most CMAs achieve higher tumor concentrations than SMs.

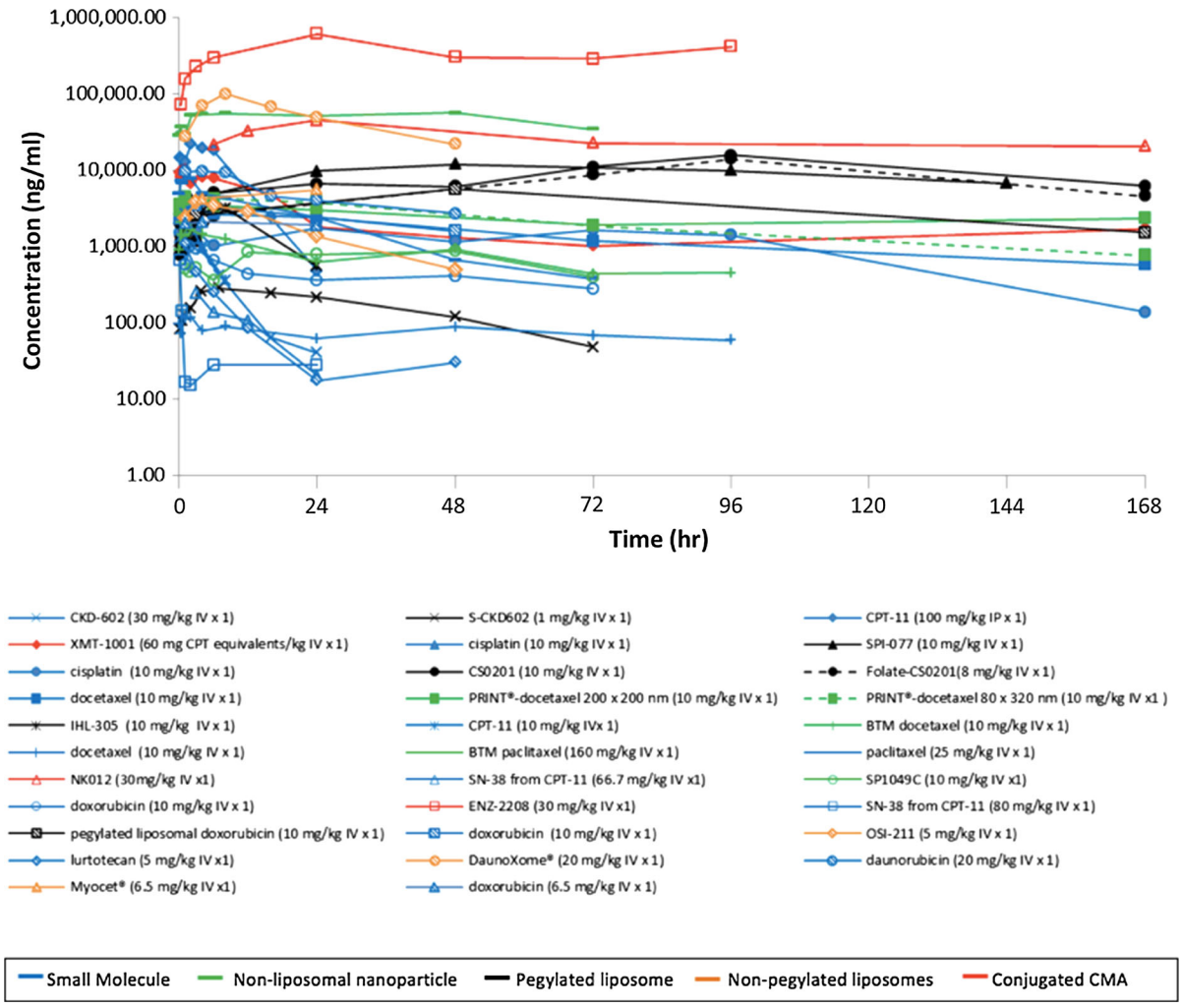


**Fig. 3** Comparison of concentration versus time profiles in tumor following the administration of CMAs and SMs. The tumor concentration versus time curves for all agents identified in the study. *Curves* with corresponding *symbols* indicate that those agents are from the same study. *Blue curves* represent SMs, *green curves* represent non-liposomal nanoparticles, *black curves* represent PEGylated lipsomes, *orange curves* represent non-PEGylated liposomes, and *red curves* represent conjugated agents. (Color figure online)

There is more variability and less systematic order seen in CMA tumor disposition than is seen in plasma, though the conjugated agents again achieve some of the highest tumor exposures. Cisplatin and docetaxel are two SMs that are detectable in tumor for an extended period of time. Cisplatin's extended exposure in tumors can be explained by its covalent binding to proteins in plasma, tumor, and tissues as described above. Docetaxel's extended duration of exposure is likely due to its formulation characteristics. Docetaxel (Taxotere®) has poor aqueous solubility and thus a surfactant, polysorbate 80, is used in the IV formulation to improve solubility (Hennenfent and Govindan 2006). This formulation leads to the formation of micelles that encapsulate docetaxel, which may give the drug CMA-like properties (van Zuylen et al. 2001). Table 2 summarizes the standard AUC data for both SMs and CMAs in plasma and tumor. The mean CMA plasma AUC was 387-fold greater than mean SM plasma AUC. Mean CMA tumor AUC was 25-fold greater than mean SM tumor AUC. The ratio of tumor AUC to plasma AUC is used as a measure of the degree of tumor delivery. The ratio of SM tumor AUC to plasma AUC divided by the ratio

**Table 2** Standard pharmacokinetics parameters for CMA and SM agents

| Agent | $AUC_{plasma}$ (ng/ml*hr) | $AUC_{tumor}$ (ng/ml*hr) | $AUC_{tumor}$/ $AUC_{plasma}$ | $(AUC_{tumor}/AUC_{plasma})_{SM}$/ $(AUC_{tumor}/AUC_{plasma})_{CMA}$ |
|---|---|---|---|---|
| CMA | | | | |
| SPI-077 | 8,369,500.0 | 1,331,400.0 | 0.2 | 4.3 |
| S CKD-602 | 201,929.0 | 13,194.0 | 0.1 | 19.6 |
| XMT-1001 | 3,307,791.0 | 541,537.0 | 0.2 | 9.0 |
| PRINT docetaxel 200 × 200 nm | 138,359.5 | 396,104.1 | 2.9 | 13.5 |
| PRINT docetaxel 80 × 320 nm | 136,416.9 | 342,937.0 | 2.5 | 15.4 |
| CS0201 | 4,590,300.0 | 1,644,300.0 | 0.4 | 15.3 |
| Folate-CS0201 | 3,243,300.0 | 1,296,700.0 | 0.4 | 13.7 |
| IHL-305 | 1,172,523.0 | 43,936.4 | 0.04 | 473.1 |
| BTM-docetaxel | 265,300.0 | 70,600.0 | 0.3 | 11.1 |
| BTM-paclitaxel | 13,718,752.0 | 3,600,767.8 | 0.3 | 7.8 |
| NK012 | 5,821,004.0 | 13,336,462.9 | 2.3 | 0.8 |
| SP1049C | 10,518.8 | 49,921.5 | 4.8 | 0.9 |
| ENZ-2208 | 90,889,572.2 | 35,400,531.0 | 0.4 | 0.7 |
| PLD | 4,225,761.4 | 564,647.8 | 0.1 | 58.9 |
| Liposomal daunorubicin | 2,096,021.1 | 2,439,618.8 | 1.2 | 22.4 |
| Liposomal doxorubicin | 96,627.6 | 109,800.0 | 1.1 | 7.7 |
| OSI-211 | 446,407.6 | 83,275.8 | 0.2 | 6.8 |
| Mean ± SD | 8,160,593.2 ± 21,632,506.6 | 2,096,021.1 ± 8,790,106.341 | 1.0 ± 1.3 | 40.1 ± 112.4 |
| Median (range) | 2,096,021.1 (10,518.8–90,889,572.2) | 541,537.0 (13,194.0–35,400,531.0) | 0.4 (0.04–4.7) | 11.1 (0.7–473.1) |
| SM | | | | |
| Cisplatin (SPI-077) | 7,200.0 | 4,900.0 | 0.7 | |
| CKD-602 (S CKD-602) | 9,117.0 | 11,661.0 | 1.3 | |
| CPT-11 (XMT-1001) | 133,754.0 | 195,991.0 | 1.5 | |
| Docetaxel (PRINT docetaxel 200 × 200 nm/ 80 × 320 nm) | 5,809.6 | 224,481.1 | 38.6 | |
| Cisplatin (CS0201/folate-CS0201) | 37,500.0 | 205,600.0 | 5.5 | |
| CPT-11 (IHL-305) | 530.3 | 9,401.0 | 17.7 | |
| Docetaxel (BTM-docetaxel) | 2,400.0 | 7,100.0 | 3.0 | |
| Paclitaxel (BTM-paclitaxel) | 73,897.0 | 151,972.1 | 2.1 | |
| SN-38 (NK012) | 1,276.4 | 2,265.6 | 1.8 | |
| Doxorubicin (SP1049C) | 7,052.7 | 29,775.3 | 4.2 | |
| SN-38 (ENZ-2208) | 2,843.9 | 796.2 | 0.3 | |
| Doxorubicin (PLD) | 15,110.0 | 118,814.3 | 7.9 | |
| Daunorubicin (liposomal daunorubicin) | 9,323.2 | 242,951.8 | 26.1 | |
| Doxorubicin (liposomal doxorubicin) | 5,488.1 | 48,116.6 | 8.8 | |
| Lurtotecan (OSI-211) | 4,598.3 | 5,852.3 | 1.3 | |
| Mean ± SD | 21,060.0 ± 36,552.3 | 83,978.6 ± 94,516.9 | 8.0 ± 11.1 | |
| Median (Range) | 7,052.7 (530.3–133,754.0) | 29,775.3 (796.2–242,951.8) | 3.0 (0.3–38.6) | |

All SM docetaxel is Taxotere®. SM paclitaxel is Taxol®. Liposomal daunorubicin is DaunoXome®. Liposomal doxorubicin is Myocet®

*PLD* pegylated liposomal doxorubicin, *SM* small molecule, *CMA* carrier mediated agent, *SD* standard deviation, $AUC_{plasma}$ area under the plasma concentration versus time curve, $AUC_{tumor}$ area under the tumor concentration versus time curve $(AUC_{tumor}/AUC_{plasma})_{SM}$ ratio of SM tumor AUC to SM plasma AUC, $(AUC_{tumor}/AUC_{plasma})_{CMA}$ ratio of CMA tumor AUC to CMA plasma AUC

of CMA tumor AUC to plasma AUC was used to directly compare the degree of tumor delivery for each formulation. A ratio value of greater than 1.0 indicates that the SM has a greater degree of tumor delivery than its comparative CMA. The mean ± SD ratio value for SM to CMA was 40.1 ± 112.4 and 14 of the 17 values

were greater than 1 suggesting SMs have a greater degree of tumor penetration compared with CMAs.

The CMAs' physiochemical properties also had an effect on their tumor PK. As was previously seen with plasma PK, the major factor affecting tumor CMA PK was PEGylation, with PEGylated agents achieving higher tumor concentrations than CMA compared with non-PEGylated agents. Particle composition played less of a role in influencing the tumor CMA PK compared with plasma PK. No other physiochemical properties were seen to affect tumor PK.

## RDI-OT PK results

The tumor to plasma RDI-OT versus time curves for all agents included in the analysis are shown in Fig. 4. SM tumor RDI-OT curves are higher than CMA RDI-OT curves from 0 to 6 h, indicating that in the hours directly after administration, SMs distribute more efficiently to tumors than CMAs. The tumor to plasma RDI-OT data for all agents is summarized in Table 3. Truncated 0–6 h RDI-OT AUCs are provided to account for the fact that SM drugs are cleared faster

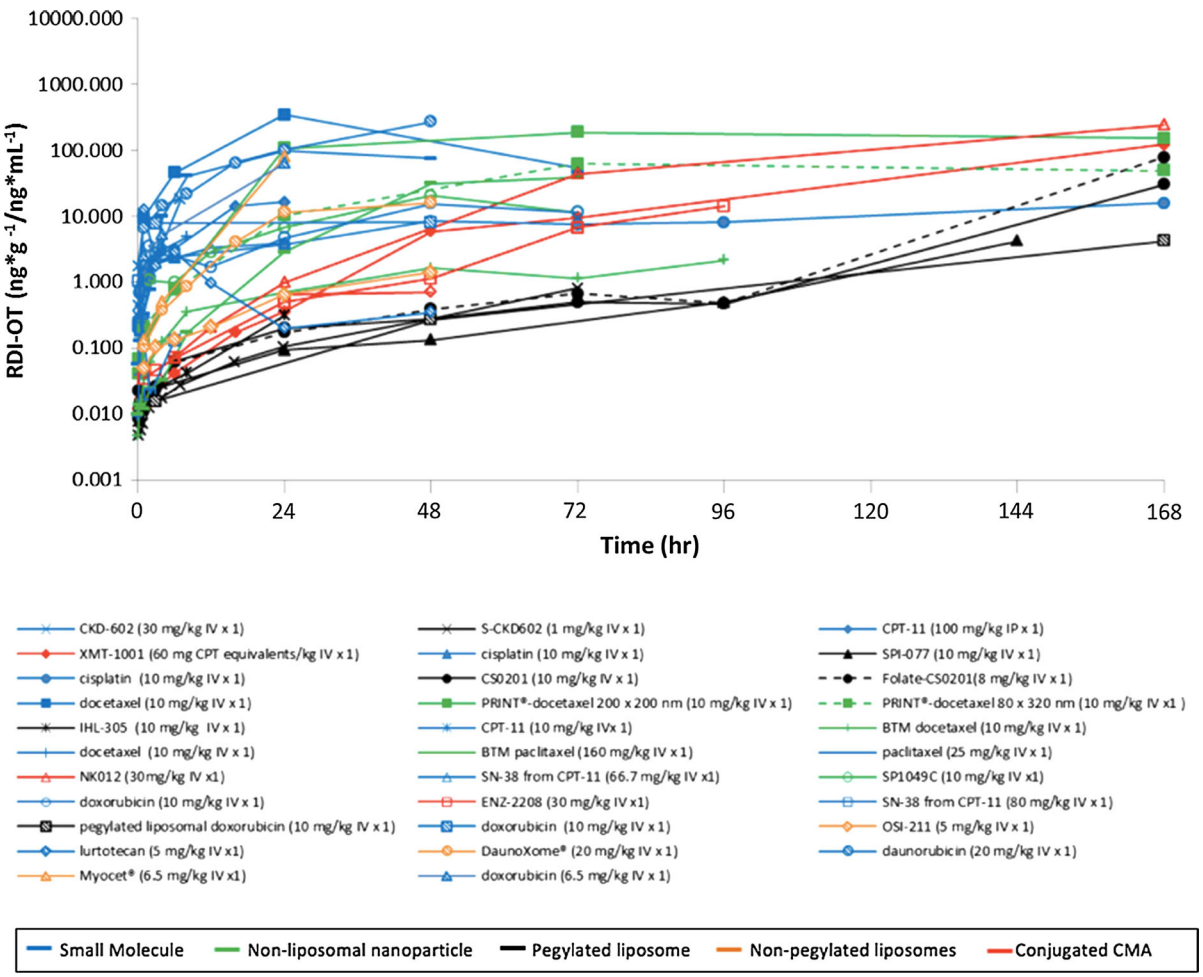


**Fig. 4** Tumor RDI-OT versus time curves following the administration of CMAs and SMs. The tumor RDI-OT versus time curves for all agents included in the study. Tumor RDI-OT is defined as the concentration of drug in tumor divided by the concentration of drug in plasma at each time point. *Curves* with corresponding *symbols* indicate that those agents are from the same study. *Blue curves* represent SMs, *green curves* represent non-liposomal nanoparticles, *black curves* represent PEGylated lipsomes, *orange curves* represent non-PEGylated liposomes, and *red curves* represent conjugated agents. (Color figure online)

**Table 3** RDI-$OT_{tumor}$ pharmacokinetic parameters for CMA and SM agents

| Agent | RDI-$OT_{tumor}$ $AUC_{0\text{-last}}$[a] | (SM RDI-$OT_{tumor}$ $AUC_{0\text{-last}}$)/(CMA RDI-$OT_{tumor}$ $AUC_{0\text{-last}}$) | RDI-$OT_{tumor}$ $AUC_{0-6\ h}$[a] | (SM RDI-$OT_{tumor}$ $AUC_{0-6\ h}$)/(CMA RDI-$OT_{tumor}$ $AUC_{0-6\ h}$) |
|---|---|---|---|---|
| CMA | | | | |
| SPI-077 | 131.3 | 0.02 | 0.02 | 98.7 |
| S CKD-602 | 18.6 | 2.1 | 0.04 | 149.3 |
| XMT-1001 | 6,488.0 | 0.03 | 0.1 | 76.1 |
| PRINT docetaxel 200X200 nm | 24,010.9 | 0.5 | 2.4 | 59.2 |
| PRINT docetaxel 80X320 nm | 7,152.7 | 1.6 | 2.5 | 55.8 |
| CS0201 | 1,131.3 | 1.3 | 0.2 | 59.5 |
| Folate-CS0201 | 2,860.5 | 0.5 | 0.2 | 63.6 |
| IHL-305 | 3.0 | 1.5 | 0.1 | 63.8 |
| BTM-docetaxel | 109.9 | 0.2 | 0.3 | 26.7 |
| BTM-paclitaxel | 1,268.2 | 2.6 | 0.1 | 129.9 |
| NK012 | 741,095.9 | $9.3 \times 10^{-5}$ | 0.1 | 87.3 |
| SP1049C | 767.9 | 0.8 | 5.2 | 2.8 |
| ENZ-2208 | 368.5 | $2.2 \times 10^{-3}$ | 0.3 | 3.1 |
| PLD | 273.8 | 1.3 | N/A | N/A |
| Liposomal daunorubicin | 414.7 | 13.4 | 0.8 | 45.4 |
| Liposomal doxorubicin | 791.9 | 0.1 | 1.0 | 12.5 |
| OSI-211 | 31.3 | 2.0 | 0.5 | 45.5 |
| Mean ± SD | 46,289.3 ± 179,143.8 | 1.7 ± 3.1 | 0.87 ± 1.40[b] | 61.2 ± 41.4 |
| Median (Range) | 767.9 (3.0–741,095.9) | 0.9 (0.00009–13.4) | 0.25 (0.02–5.2) | 59.4 (2.8–149.3) |
| SM | | | | |
| Cisplatin (SPI-077) | 2.3 | | 2.3 | |
| CKD-602 (S CKD-602) | 39.0 | | 6.6 | |
| CPT-11 (XMT-1001) | 219.4 | | 11.1 | |
| Docetaxel (PRINT docetaxel 200 × 200 nm/80 × 320 nm) | 11,057.7 | | 141.9 | |
| Cisplatin (CS0201/folate-CS0201) | 1,443.1 | | 11.0 | |
| CPT-11 (IHL-305) | 4.5 | | 4.5 | |
| Docetaxel (BTM-docetaxel) | 22.5 | | 6.7 | |
| Paclitaxel (BTM-paclitaxel) | 3,292.0 | | 11.3 | |
| SN-38 (NK012) | 68.9 | | 9.3 | |
| Doxorubicin (SP1049C) | 628.2 | | 14.5 | |
| SN-38 (ENZ-2208) | 0.8 | | 0.8 | |
| Doxorubicin (PLD) | 366.5 | | N/A | |
| Daunorubicin (liposomal daunorubicin) | 5,568.4 | | 34.9 | |
| Doxorubicin (liposomal doxorubicin) | 700.0 | | 12.9 | |
| Lurtotecan (OSI-211) | 61.6 | | 24.0 | |
| Mean ± SD | 1,565.0 ± 3,053.6 | | 20.8 ± 36.0 | |
| Median (Range) | 144.1 (0.8–11,057.7) | | 11.1 (0.8–141.9) | |

All SM docetaxel is Taxotere®. SM paclitaxel is Taxol®. Liposomal daunorubicin is DaunoXome®. Liposomal doxorubicin is Myocet®

*PLD* pegylated liposomal doxorubicin, *SM* small molecule, *CMA* carrier mediated agent, *SD* standard deviation, *RDI-$OT_{tumor}$ $AUC_{0-last}$* area under the tumor relative distribution index-over time versus time curve from 0 h to last pharmacokinetic time point, *RDI-$OT_{tumor}$ $AUC_{0-6\ h}$* area under the tumor relative distribution index-over time versus time curve from 0 to 6 h

[a] Units: $(ng*g^{-1}/ng*mL^{-1})*h$

[b] Different from SM ($P < 0.05$)

than CMAs and therefore cannot have RDI-OT values at later time points. The ratio of SM RDI-OT $AUC_{0–last}$ value to comparative CMA RDI-OT $AUC_{0-last}$ value was calculated for all agents. In addition, the ratio of SM RDI-OT $AUC_{0–6\ h}$ value to comparative CMA RDI-OT $AUC_{0–6\ h}$ value was also calculated for all the agents. These parameters were used to directly compare the efficiency of tumor delivery between SM and CMA. Ratio values greater than 1.0 indicate that SMs have more efficient tumor delivery than their comparative CMA. Eight of the 17 (48 %) SM RDI-OT $AUC_{0–last}$ to comparative CMA RDI-OT $AUC_{0–last}$ ratios were greater than 1.0. In addition, 16 of the 16 SM RDI-OT $AUC_{0–6\ h}$ to comparative CMA RDI-OT $AUC_{0–6\ h}$ ratios were greater than 1.0. These results indicate that the majority of SMs have more efficient delivery to tumor compared to their comparative CMA, especially in the hours directly after administration.

RDI-OT $AUC_{0–last}$ and RDI-OT $AUC_{0–6\ h}$ for both liver and spleen are summarized in Table 4. Six of 14 SMs have a greater liver RDI-OT $AUC_{0–last}$ than their comparative CMA, while all SMs have a greater liver RDI-OT $AUC_{0–6\ h}$ than their comparative CMA. Three of 12 SMs have a greater spleen RDI-OT $AUC_{0–last}$ than their comparative CMA, while all SMs have a greater spleen RDI-OT $AUC_{0–6\ h}$ than their comparative CMA. The results of liver and spleen RDI-OT are more variable than that of tumor. However, when RDI-OT AUCs are measured to 6 h, all SMs in both liver and spleen achieve greater RDI-OT AUCs than their comparative CMA.

### Comparison of standard and RDI-OT PK parameters

The association between RDI-OT AUC and ratio of tissue or tumor AUC to plasma AUC for both CMAs and SMs is shown in Fig. 5. There is no association between RDI-OT AUC and ratio of tissue AUC to plasma AUC for either SMs or CMAs in any tissue, with the exception for SM in tumor ($R = 0.87$). However, the association of RDI-OT AUC and ratio of tumor AUC to plasma AUC for SM appears to be driven by the presence of two outliers, as when these two outliers are removed no association is observed ($R = -0.0436$). The lack of association between RDI-OT AUC and AUC ratio in both tumor and tissues suggest that that RDI-OT is a novel PK parameter that is independent from tumor or tissue AUC to plasma AUC ratio and thus is measuring a different PK principle.

## Discussion

The evaluation of the PKs of CMAs relative to SMs has been limited due to the lack of development of PK metrics and parameters that evaluate the degree and efficiency of distribution to tissues and especially tumors. Thus, we developed a novel PK parameter called RDI-OT that evaluates the efficiency of delivery of CMAs and SMs to tumors and tissues. CMAs have much greater plasma exposure compared to SMs due to their long residence time in the plasma, which is easily seen when the plasma concentration versus time curves and AUCs of CMAs are compared with those of SMs. The tumor AUCs of CMAs are also higher than the tumor AUCs of SMs, presumably due to the EPR effect (Duncan 1999; Zamboni 2005, 2008). However, using RDI-OT, we have shown that in mice with flank subcutaneous human xenograft and flank synergistic tumors, SMs distribute into tumor more efficiently than CMAs. In addition, 14 of 17 (82 %) SMs have a greater tumor AUC to plasma AUC ratio than their comparative CMA. While SMs are cleared from plasma much faster than CMAs the proportion of tumor drug exposure relative to plasma drug exposure is greater for SMs compared to CMAs. In addition, every small SM tumor RDI-OT $AUC_{0–6\ h}$ value is greater than that of its comparative CMA. This suggests that tumor distribution of CMAs is less efficient than SMs. The reason for lower efficiency of CMA tumor delivery compared to SMs is unclear.

Liver and spleen had more variable RDI-OT results than tumor. Only a quarter of SMs managed to achieve a greater RDI-OT $AUC_{0–last}$ than their comparative CMA in spleen and only 6 of 14 (43 %) SMs achieved a greater RDI-OT $AUC_{0–last}$ than their comparative CMA in liver. However, this is to be expected as CMAs have a much longer exposure than SMs and therefore can have RDI-OT values calculated out to much later time points. When RDI-OT AUC values are truncated to 6 h, liver results start to fall in line with the tumor results, with all SMs achieving a greater liver RDI-OT $AUC_{0–6\ h}$ than their comparative CMA. Truncating spleen RDI-OT AUC values to 6 h produces the same results, with all SMs achieving a

**Table 4** Tissue RDI-OT pharmacokinetic parameters for CMA and SM agents

| Agent | RDI-$OT_{liver}$ $AUC_{0–last}$[a] | RDI-$OT_{liver}$ $AUC_{0–6\ h}$[a] | RDI-$OT_{spleen}$ $AUC_{0–6\ h}$[a] | RDI-$OT_{spleen}$ $AUC_{0–6\ h}$[a] |
|---|---|---|---|---|
| CMA | | | | |
| SPI-077 | 392.9 | 0.1 | 1,117.7 | 0.1 |
| S CKD-602 | 11.62 | 0.4 | 46.1 | 0.3 |
| XMT-1001 | 26,188 | 1.0 | 14,915.0 | 0.4 |
| PRINT docetaxel 200X200 | 11,917.6 | 3.0 | 112,966.7 | 21.9 |
| PRINT docetaxel 80X320 | 526.5 | 1.6 | 2,292.0 | 9.8 |
| CS0201 | 488 | 0.6 | 3,428.0 | 0.7 |
| Folate-CS0201 | 5,707 | 1.4 | 4,130.0 | 0.8 |
| IHL-305 | 4.5 | 0.3 | 9.3 | 0.4 |
| BTM-docetaxel | 906.9 | 13.3 | 303.7 | 6.3 |
| BTM-paclitaxel | 42,118.5 | 1.2 | 56,669.6 | 1.4 |
| NK012 | 2,833,721.1 | 0.9 | 5,152,753.6 | 0.7 |
| SP1049C | 1,167.2 | 50.0 | N/A | N/A |
| ENZ-2208 | N/A | N/A | N/A | N/A |
| PLD | 367.0 | N/A | N/A | N/A |
| Liposomal daunorubicin | N/A | N/A | N/A | N/A |
| Liposomal doxorubicin | N/A | N/A | N/A | N/A |
| OSI-211 | 38.4 | 1.8 | 204.2 | 2.5 |
| Mean ± SD | 208,825.4 ± 755,599.6 | 5.8 ± 13.7[b] | 445,736.3 ± 1,482,716.5 | 3.8 ± 6.43[b] |
| Median (Range) | 1,416,862.8 (4.5–2,833,721.1) | 1.2 (0.1–50.0) | 2,860.0 (9.3–5,152,753.6) | 0.75 (0.1–21.9) |
| SM | | | | |
| Cisplatin (SPI-077) | 8.9 | 9.0 | 1.7 | 1.7 |
| CKD-602 (S CKD-602) | 96.0 | 40.0 | 22.1 | 10.6 |
| CPT-11 (XMT-1001) | 490.6 | 68.8 | 917.7 | 83.0 |
| Docetaxel (PRINT docetaxel 200 × 200 nm/80 × 320 nm) | 127.8 | 22.4 | 186.2 | 42.0 |
| Cisplatin (CS0201/folate-CS0201) | 2,743.0 | 17.0 | 647.0 | 2.1 |
| CPT-11 (IHL-305) | 14.4 | 28.4 | 27.7 | 34.5 |
| Docetaxel (BTM-docetaxel) | 83.3 | 39.0 | 535.7 | 201.5 |
| Paclitaxel (BTM-paclitaxel) | 2,240.0 | 42.4 | 969.8 | 9.3 |
| SN-38 (NK012) | 107.9 | 26.1 | 10.3 | 2.2 |
| Doxorubicin (SP1049C) | 1,534.7 | 72.5 | N/A | N/A |
| SN-38 (ENZ-2208) | N/A | N/A | N/A | N/A |
| Doxorubicin (PLD) | 409.8 | N/A | N/A | N/A |
| Daunorubicin (liposomal doxorubicin) | N/A | N/A | N/A | N/A |
| Doxorubicin (liposomal doxorubicin) | N/A | N/A | N/A | N/A |
| Lurtotecan (OSI-211) | 271.0 | 85.4 | 230.6 | 100.4 |
| Mean ± SD | 677.3 ± 949.6 | 41 ± 24.6 | 354.9 ± 382.7 | 48.73 ± 64.1 |
| Median (Range) | 199.4 (8.9–2,743.0) | 39 (9.0–85.4) | 208.4 (1.7–969.8) | 22.6 (1.7–201.5) |

All SM docetaxel is Taxotere®. SM paclitaxel is Taxol®. Liposomal daunorubicin is DaunoXome®. Liposomal doxorubicin is Myocet®

*PLD* pegylated liposomal doxorubicin, *SM* small molecule, *CMA* carrier mediated agent, *SD* standard deviation, *RDI-$OT_{tumor}$ $AUC_{0–last}$* area under the tumor relative distribution index-over time versus time curve from 0 h to last pharmacokinetic time point, *RDI-$OT_{tumor}$ $AUC_{0–6\ h}$* area under the tumor relative distribution index-over time versus time curve from 0 to 6 h

[a] Units: $(ng*g^{-1}/ng*mL^{-1})*h$

[b] Different from SM ($P < 0.05$)

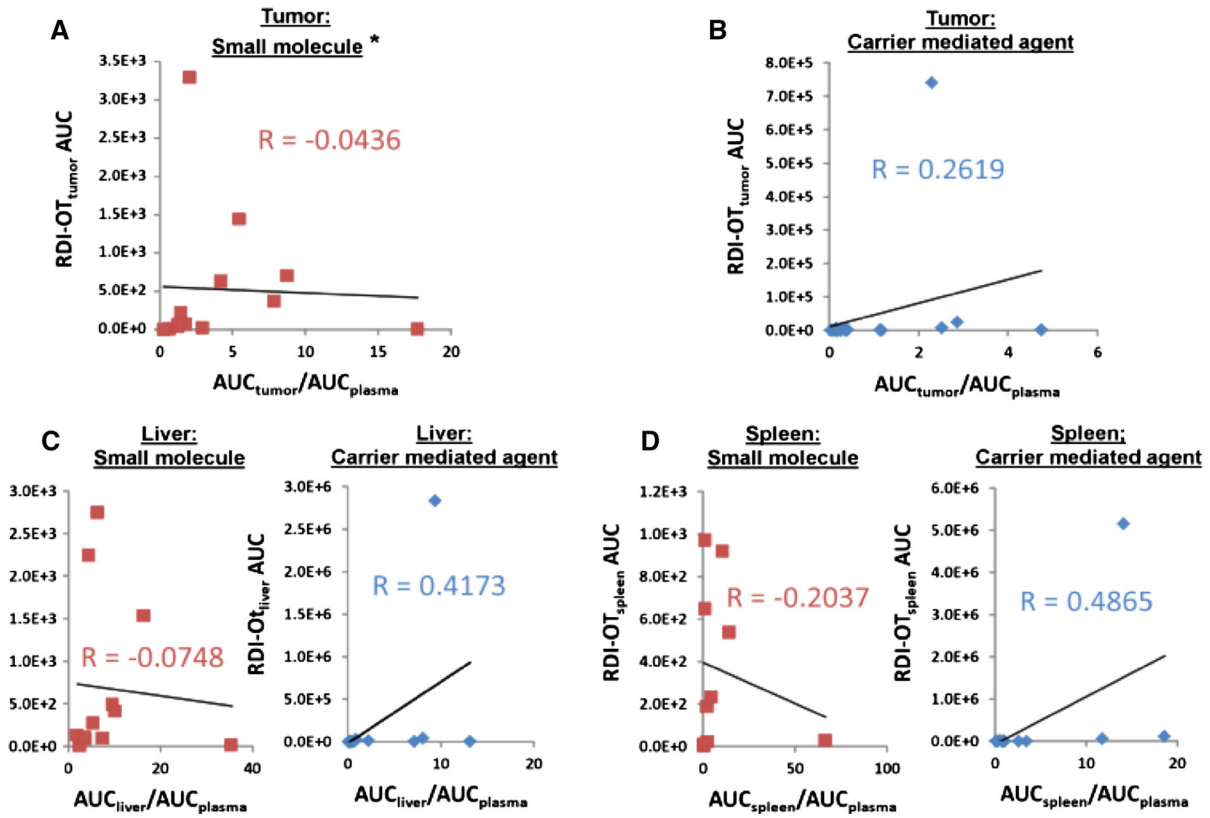


**Fig. 5** Association between RDI-OT AUC in tumor and tissues, and ratio of tumor AUC or tissue AUC to plasma AUC for CMA and SM. **a** Association between SM RDI-$OT_{tumor}$ $AUC_{0–last}$ [(ng*$g^{-1}$/ng*$mL^{-1}$)*h] and SM tumor AUC to plasma AUC ratio. Two outliers have been removed. **b** Association between CMA RDI-$OT_{tumor}$ $AUC_{0–last}$ [(ng*$g^{-1}$/ng*$mL^{-1}$)*h] and CMA tumor AUC to plasma AUC ratio. **c** Association between RDI-$OT_{liver}$ $AUC_{0–last}$ [(ng*$g^{-1}$/ng*$mL^{-1}$)*h] and liver AUC to plasma AUC ratio. SMs (*red*) and CMAs (*blue*) have been compared separately. **d** Association between RDI-$OT_{spleen}$ $AUC_{0–last}$ [(ng*$g^{-1}$/ng*$mL^{-1}$)*h] and spleen AUC to plasma AUC ratio. SMs (*red*) and CMAs (*blue*) have been compared separately. *Two outliers have been removed. $R = 0.8653$ with outliers included. (Color figure online)

greater spleen RDI-OT $AUC_{0–6\ h}$ than their comparative CMA.

RDI-OT is a new PK metric to evaluate the efficiency of drug delivery from plasma to tumor and tissues. The purpose of RDI-OT is not to bypass circulation ability; rather it is to evaluate the ability of CMAs and SMs to penetrate into tumor from circulation. By evaluating the relationship between plasma drug concentration and tumor or tissue drug concentration, we attempted to demonstrate that high plasma drug concentrations do not necessarily result in continually rising tumor and tissue concentrations. Logically, it would be expected that while plasma concentrations are high, tumor and tissue drug concentrations would continue to increase. Using RDI-OT, we have shown that this is not necessarily the case. A high plasma concentration combined with low tumor/tissue concentration is indicative of inefficient tissue/tumor delivery and results in a low RDI-OT value which corresponds with low efficiency. RDI-OT is different from the ratio of tissue or tumor AUC to plasma AUC because there are no tumor, tissue, or plasma AUC values used in the calculation of RDI-OT. Rather, the ratio of drug concentration in tumor or tissue to drug concentration in plasma is calculated at each individual time point. Once these calculations are made, they can be plotted against time and the AUC can be calculated creating the RDI-OT AUC. Furthermore, when RDI-OT AUCs were compared to ratios of tissue or tumor AUC to plasma AUC, there was no

association between these values for either CMAs or SMs in all the tissues observed. In addition to the mathematical differences between RDI-OT and ratio of tumor AUC to plasma AUC, RDI-OT provides several additional unique results that AUC calculations do not. First, RDI-OT can assess the efficiency of the ability of SMs and CMAs to enter tissues and tumor from plasma, whereas AUC ratio is only a relative measure of the total drug exposure between plasma and tumor or tissues. Second, RDI-OT values are calculated for each time point and thus it is possible to evaluate the efficiency of a SM or CMA drug at single time point and at various time points, while AUC ratio can only measure the total exposure over the total period of time. Thus, RDI-OT is a novel PK metric that can be used to evaluate the efficiency of delivery of CMAs and SMs to tumors and tissues.

While RDI-OT is a novel PK metric, it has not yet been correlated to pharmacodynamics (PD) effects. Future studies should be performed to determine what effect RDI-OT has on PD outcomes. It would be useful to see how RDI-OT values correlates to tumor regression as well as overall survival. These studies will be important to determine how RDI-OT relates to the efficacy of both CMA and SM agents.

The results of this study do give us novel insights into the plasma, tissue, and especially tumor PK disposition of CMAs; however, there are some limitations. All of the tumor models studied in this analysis were subcutaneous flank xenografts. Recent studies have shown that the PK of carboplatin in genetically engineered mouse models (GEMMs) of melanoma more closely resembles the tumor disposition of carboplatin seen in patient with cutaneous tumors when compared to other transplanted melanoma tumor models (Combest et al. 2012). The combination of the results from the study by Combest et al. (2012), and our current study suggest that flank tumor models may not be optimal to evaluate the tumor delivery and efficacy of CMAs. However, the comparison of the tumor delivery of CMAs and SMs in several types of tumors models and in patients with solid tumors needs to be performed to confirm these results. In addition, our current study may need to be repeated in models which more closely resemble tumors seen in patients, such as orthotopic or GEMMs.

An additional limitation of this study was that the total (encapsulated + released) concentration of CMAs was compared to the concentration of their comparator SMs. Ideally, we would have compared the concentration of encapsulated and released drug from CMAs to the concentrations of their comparator SMs. To more thoroughly evaluate the plasma and tumor disposition of CMAs, it would be best to evaluate encapsulated and released drug in plasma and tumor. However, most of these studies were performed before methods were available to measure encapsulated and released drug in plasma. In addition, it is still very difficult to measure encapsulated and released drug in tumor and other tissues, as most methods for measuring drug concentrations in tissue cause the encapsulated drug to be released during the process. However, this limitation of our study does highlight the need to develop novel methods to measure encapsulated and released drug in plasma, tumor, and tissues for all CMAs.

Lastly, the results from this study could be interpreted differently depending on one's views concerning the mechanism of CMA drug delivery. Contradictory to current theories for CMA tumor delivery, which suggest that CMAs preferentially accumulate in the tumor prior to releasing their contents; it is possible that CMAs do not accumulate in the tumor at all. Instead, tumor drug exposure could be related only to the drug that is released from the carrier into the blood and is then distributed to the tumor as free SM drug. If this alternative theory is the primary mechanism of tumor drug delivery, it is possible that the RDI-OT values of CMAs are lower than those of SMs, not because they distribute into the tissues less efficiently than SMs, but rather because CMAs release their contents from the carrier into the blood stream at a very low rate. This potential alternative theory also highlights the need to develop methods to evaluate encapsulated and released drug in blood, plasma, tumor, and tissues.

## Conclusion

We have developed a new PK metric, RDI-OT, for the evaluation of the efficiency of tumor and tissue drug delivery of SMs and CMA drugs. Using this metric, we have demonstrated that the efficiency of CMA tumor delivery is lower than that of SM drugs in mice bearing subcutaneous flank synergistic and xenograft tumors. Additional studies are needed to evaluate if these results are reproducible in additional tumor models. In

addition, new methods, technologies, and model systems are needed to improve the efficiency by which CMAs are delivered to and penetrate into tumors.

**Conflict of interest** Research reported in this publication was supported by the National Cancer Institute of the National Institutes of Health under Award Number U54CA151652. The content is solely the responsibility of the authors and does not necessarily represent the official views of the National Institutes of Health.

## References

Alakhov V, Klinski E, Li S, Pietrzynski G, Venne A, Batrakova E et al (1999) Block copolymer-based formulation of doxorubicin. From cell screen to clinical trials. Colloids Surf B 16:113–134

Alonso MJ (2004) Nanomedicines for overcoming biological barriers. Biomed Pharmacother 58:168–172

Caron WP, Song G, Kumar P, Rawal S, Zamboni WC (2012) Interpatient pharmacokinetic and pharmacodynamic variability of carrier-mediated anticancer agents. Clin Pharmacol Ther 91:802–812

Chu KS, Hasan W, Rawal S, Walsh MD, Enlow EM et al (2013) Plasma, tumor and tissue pharmacokinetics of docetaxel delivered via nanoparticles of different sizes and shapes in mice bearing SKOV-3 human ovarian carcinoma xenograft. Nanomedicine 9:686–693

Combest AJ, Roberts PJ, Dillon PM, Sandison K, Hanna SK et al (2012) Genetically engineered cancer models, but not xenografts, faithfully predict anticancer drug exposure in melanoma tumors. Oncologist 17:1303–1316

Desjardins JP, Abbott EA, Emerson DL, Tomkinson BE, Leray JD, Brown EN et al (2001) Biodistribution of NX211, liposomal lurtotecan, in tumor-bearing mice. Anticancer Drugs 12:235–245

Drummond DC, Meyer O, Hong K, Kirpotin DB, Papahadjopoulos D (1999) Optimizing liposomes for delivery of chemotherapeutic agents to solid tumors. Pharmacol Rev 51:691–743

Duncan R (1999) Polymer conjugates for tumour targeting and intracytoplasmic delivery. The EPR effect as a common gateway? Pharm Sci Technol Today 2:441–449

Farrell NP (2011) Platinum formulations as anticancer drugs clinical and pre-clinical studies. Curr Top Med Chem 11:2623–2631

Feng L, Benhabbour SR, Mumper RJ (2013) Oil-filled lipid nanoparticles containing 2′-(2-bromohexadecanoyl)-docetaxel for the treatment of breast cancer. Adv Healthc Mater 2:1451–1457

Forssen EA, Coulter DM, Proffitt RT (1992) Selective in vivo localization of daunorubicin small unilamellar vesicles in solid tumors. Cancer Res 52:3255–3261

Gabizon Goren D, Horowitz T, Tzemach A, Losos A, Siegal T et al (1997) Long-circulating liposomes for drug delivery in cancer therapy: a review of biodistribution studies in tumor-bearing animals. Adv Drug Deliv Rev 24:337–344

Ge Y, Tiwari A, Li S (2011) Nanomedicine—bridging the gap between nanotechnology and medicine. Adv Mat Lett 2:1–2

Hennenfent KL, Govindan R (2006) Novel formulations of taxanes: a review. Old wine in a new bottle? Ann Oncol 17:735–749

Konishi H, Takagi A, Kurita A, Kaneda N, Matsuzaki T (2012) PEGylated liposome IHL-305 markedly improved the survival of ovarian cancer peritoneal metastasis in mouse. BMC Cancer 12:462

Laverman P, Carstens MG, Boerman OC, Dams ET, Oyen WJ, van Rooijen N, Corstens FH, Storm G (2001) Factors affecting the accelerated blood clearance of polyethylene glycol-liposomes upon repeated injection. J Pharmacol Exp Ther 298:607–612

Litzinger DC, Buiting AM, van Rooijen N, Huang L (1994) Effect of liposome size on the circulation time and intraorgan distribution of amphipathic poly(ethylene glycol)-containing liposomes. Biochim Biophys Acta 1190:99–107

Ma P, Rahima Benhabbour S, Feng L, Mumper RJ (2013) 2′-Behenoyl-paclitaxel conjugate containing lipid nanoparticles for the treatment of metastatic breast cancer. Cancer Lett 334:253–262

Matsumura Y, Maeda H (1986) A new concept for macromolecular therapeutics in cancer chemotherapy: mechanism of tumoritropic accumulation of proteins and the antitumor agent smancs. Cancer Res 46:6387–6392

Mayer LD, Bally MB, Cullis PR, Wilson SL, Emerman JT (1990) Comparison of free and liposome encapsulated doxorubicin tumor drug uptake and antitumor efficacy in the SC115 murine mammary tumor. Cancer Lett 53:183–190

Oberoi HS, Nukolova NV, Laquer FC, Poluektova LY, Huang J et al (2012) Cisplatin-loaded core cross-linked micelles: comparative pharmacokinetics, antitumor activity, and toxicity in mice. Int J Nanomedicine 7:2557–2571

Papahadjopoulos D, Allen TM, Gabizon A, Mayhew E, Matthay K, Huang SK, Lee KD, Woodle MC, Lasic DD, Redemann C et al (1991) Sterically stabilized liposomes: improvements in pharmacokinetics and antitumor therapeutic efficacy. Proc Natl Acad Sci USA 88:11460–11464

Sapra P, Zhao H, Mehlig M, Malaby J, Kraft P, Longley C et al (2008) Novel delivery of SN38 markedly inhibits tumor growth in xenografts, including a camptothecin-11-refractory model. Clin Cancer Res 14:1888–1896

Takahashi A, Ohkohchi N, Yasunaga M, Kuroda J, Koga Y, Kenmotsu H et al (2010) Detailed distribution of NK012, an SN-38-incorporating micelle, in the liver and its potent antitumor effects in mice bearing liver metastases. Clin Cancer Res 16:4822–4831

van Zuylen L, Verweij J, Sparreboom A (2001) Role of formulation vehicles in taxane pharmacology. Invest New Drugs 19:125–141

Vonarbourg A, Passirani C, Saulnier P, Benoit JP (2006) Parameters influencing the stealthiness of colloidal drug delivery systems. Biomaterials 27:4356–4373

Walsh MD, Hanna SK, Sen J, Rawal S, Cabral CB et al (2012) Pharmacokinetics and antitumor efficacy of XMT-1001, a novel, polymeric topoisomerase I inhibitor, in mice bearing HT-29 human colon carcinoma xenografts. Clin Cancer Res 18:2591–2602

Zamboni WC (2005) Liposomal, nanoparticle, and conjugated formulations of anticancer agents. Clin Cancer Res 11:8230–8234

Zamboni WC (2008) Concept and clinical evaluation of carrier-mediated anticancer agents. Oncologist 13:248–260

Zamboni WC, Gervais AC, Egorin MJ, Schellens JH, Zuhowski EG et al (2004) Systemic and tumor disposition of platinum after administration of cisplatin or STEALTH liposomal-cisplatin formulations (SPI-077 and SPI-077 B103) in a preclinical tumor model of melanoma. Cancer Chemother Pharmacol 53:329–336

Zamboni WC, Strychor S, Joseph E, Walsh DR, Zamboni BA et al (2007) Plasma, tumor, and tissue disposition of STEALTH liposomal CKD-602 (S-CKD602) and nonliposomal CKD-602 in mice bearing A375 human melanoma xenografts. Clin Cancer Res 13:7217–7223